# Elastic scattering of electrons from Xe, $Cs^+$, and $Ba^{2+}$

W. R. Johnson
*Department of Physics, University of Notre Dame, Notre Dame, Indiana 46556*

C. Guet
*Commissariat à l'Énergie Atomique, Département de Recherche Fondamentale Matière Condensée, Laboratorie d'Ions Atomes et Agrégats, Centre d'Etudes Nucléaires de Grenoble, 85X, 38041 Grenoble Cedex, France*

(Received 7 September 1993)

Relativistic many-body perturbation theory is applied to study the elastic scattering of electrons from xenon and from the xenonlike ions $Cs^+$ and $Ba^{2+}$, below their respective inelastic thresholds. The quasiparticle equation for the electron scattering wave function is solved in second-order perturbation theory starting from the Hartree-Fock approximation. Phase shifts for partial waves with $\ell = 0$–5 are determined as functions of electron momentum for each ion. The theoretical elastic scattering cross section for xenon is found to be in agreement with experiment, showing a Ramsauer-Townsend minimum below 1 eV. Agreement with experiment is also found for differential cross sections and scattering asymmetry functions for xenon. Differential cross sections and scattering asymmetry functions for $Cs^+$ and $Ba^{2+}$ are predicted at 10 eV.

PACS number(s): 34.80.Bm, 34.80.Nz, 31.20.Tz, 11.80.−m

## I. INTRODUCTION

Although low-energy scattering of electrons from closed-shell atoms has been a subject for experimental [1–3] and theoretical [4,5] investigation for more than 60 years, relatively little work has been done on the related problem of low-energy elastic scattering from ions. A characteristic feature of low-energy scattering of electrons from noble-gas atoms is the existence of a sharp minimum in the cross section at electron energies $< 1$ eV; the Ramsauer-Townsend minimum. This feature of the cross section is a manifestation of the polarization of the atomic core by the scattered electron; to account for it theoretically, one must include effects of electron correlation. In recent years a number of more or less sophisticated calculations describing low-energy scattering from xenon have appeared. These include the calculations of McEachran and Stauffer [6–8], who account for correlation using an optical potential; the calculations of Yuan and Zhang [9], who use the polarization potential of Padial and Norcross [10]; and those of Sienkiewicz and Baylis [11], who include correlation using a two-parameter polarization potential with exchange. All of these recent calculations account for the Ramsauer-Townsend minimum in the observed spectrum and for the observed low-energy differential cross sections.

The present work starts with yet another calculation of low-energy electron-xenon scattering. This calculation can be considered as a kind of theoretical benchmark for our treatment of correlation in ions. The electron-xenon scattering calculation is followed by calculations for xenonlike ions made using identical methods. These calculations are carried out relativistically, since xenon and the xenonlike ions under consideration have high nuclear charge, leading to observable fine-structure effects. We employ many-body perturbation theory to account for the effects of electron correlation. In lowest order, we approximate the scattering wave function by a continuum Hartree-Fock (HF) wave function in the spherically symmetrical $V^{(N-1)}$ potential of the atomic (or ionic) core. The scattered electron polarizes the core, thereby modifying the HF potential. The correction to the HF potential induced by the scattered electron is the electron self-energy; the sum of the HF potential and the electron self-energy defines an optical potential. The interaction of the electron with the optical potential is governed by a single-particle equation, the quasiparticle equation. In the present work, we calculate the electron self-energy and solve the quasiparticle equation in second-order perturbation theory. Our treatment of correlation is similar to that of Pindzola and Kelly [12], who carried out calculations of low-energy electron-argon elastic scattering in an optical potential determined from nonrelativistic many-body perturbation theory. It is also closely related to the many-body calculations of Amusia *et al.* [13,14] on elastic scattering of electrons from helium, argon, and xenon.

For xenon, the Hartree-Fock phase shifts, as well as the quasiparticle phase shifts, agree with the predictions of Levinson's theorem: the zero-momentum phase shifts for angular momentum $\kappa$ are related to $n_\kappa$, the number of occupied bound states with angular momentum $\kappa$, by the equation $\delta_\kappa(0) = n_\kappa \pi$. The slope of the $s$-wave phase shift for xenon predicted by HF calculations is negative at $p = 0$; however, after adding correlation corrections, the slope becomes positive. The phase shift increases from its threshold value to a maximum near 0.15 eV and then decreases, passing through its threshold value again at about 0.7 eV, leading to the observed Ramsauer-Townsand minimum in the cross section near that energy.

The cross section evaluated with correlated phase shifts

 

is found to be in good agreement with experimental measurements. Differential cross sections for xenon are also calculated and compared with experiment; again, the correlated values agree well with observations. Comparison of theory with experiment is, however, less satisfactory for the Sherman asymmetry function. Generally, the comparison between theory and experiment for xenon is good, encouraging us to use the same many-body techniques to study scattering from xenonlike ions.

For xenonlike ions, the phase shifts near zero momentum are the sum of the ionic Coulomb phase shifts and short-range phase shifts caused by the interaction of the scattering electron with the core electrons. At zero momentum, these later phase shifts are related to $\mu_\kappa$, the quantum defects determined from the bound-state spectra, by $\delta_\kappa(0) = \pi\mu_\kappa$. The correlated phase shifts for $Cs^+$ and $Ba^{2+}$ at $p = 0$ agree very well with values from quantum defect analyses, except for the $f$-wave phase shifts in $Ba^{2+}$, where penetration of the $4f$ orbital into the core leads to a breakdown of perturbation theory. For this particular partial wave, a phenomenological method for evaluating the phase shifts is adopted.

Differential cross sections and Sherman asymmetry functions are given at 10 eV for both ions. To our knowledge, no measurements of these quantities at low energies are available; however, we hope that the present calculations will encourage low-energy electron-ion elastic scattering experiments.

## II. DESCRIPTION OF METHOD

The scattering of a relativistic electron from a central potential is governed by two amplitudes: the *no spin-flip* amplitude $f(\theta)$, and the *spin-flip* amplitude $g(\theta)$ [15]. These amplitudes are given in terms of scattering phase shifts $\delta_\kappa(p)$, where $\kappa$ is the relativistic angular momentum quantum number ($\kappa = -\ell - 1$ for $j = \ell + 1/2$ and $\kappa = \ell$ for $j = \ell - 1/2$), by the formulas

$$f(\theta) = \frac{1}{2ip}\sum_{\ell=0}^{\infty}[(\ell+1)(e^{2i\delta_{-\ell-1}}-1) + \ell(e^{2i\delta_\ell}-1)]P_\ell(\cos\theta) \tag{2.1}$$

and

$$g(\theta) = \frac{1}{2ip}\sum_{\ell=1}^{\infty}(e^{2i\delta_{-\ell-1}} - e^{2i\delta_\ell})P_\ell^1(\theta)\,. \tag{2.2}$$

The differential scattering cross section is expressed in terms of $f(\theta)$ and $g(\theta)$ by

$$\frac{d\sigma}{d\Omega} = |f(\theta)|^2 + |g(\theta)|^2\,, \tag{2.3}$$

and the left-right scattering asymmetry function (Sherman function) is given by [16]

$$S(\theta) = \frac{2\,\mathrm{Im}[f(\theta)g^*(\theta)]}{|g(\theta)|^2 + |f(\theta)|^2}\,. \tag{2.4}$$

The problem of describing low-energy scattering is thus reduced to the problem of determining the elastic scattering phase shifts $\delta_\kappa(p)$ as functions of electron momentum.

Our point of departure for determining these phase shifts is the relativistic quasiparticle equation for the scattered electron,

$$(h + V_{\rm HF} + \Sigma_\varepsilon)\phi_{\varepsilon\kappa} = \varepsilon\phi_{\varepsilon\kappa}\,, \tag{2.5}$$

which is obtained from Dyson's equation for the one-particle Green's function [17]. In Eq. (2.5), $h$ is the single-particle Dirac Hamiltonian

$$h = c\,\boldsymbol{\alpha}\cdot\boldsymbol{p} + \beta mc^2 - \frac{e^2Z}{r}\,, \tag{2.6}$$

$V_{\rm HF}$ is the (Dirac) Hartree-Fock potential for the closed-shell atom or ion, and $\Sigma_\varepsilon$ is the electron self-energy (or polarization) operator.

In lowest order, we neglect $\Sigma_\varepsilon$ in Eq. (2.5) and solve the resulting continuum HF equation to find an approximate scattering wave function $\phi^{\rm HF}_{\varepsilon\kappa}(\mathbf{r})$. The corresponding phase shift is designated by $\delta^{\rm HF}_\kappa(p)$. The lowest nonvanishing correlation correction to this wave function, $\Delta\phi_{\varepsilon\kappa}$, is found by solving the inhomogeneous equation obtained from Eq. (2.5), treating $\Sigma_\varepsilon$ as a perturbation:

$$(h + V_{\rm HF} - \varepsilon)\Delta\phi_{\varepsilon\kappa} = -\Sigma_\varepsilon\phi^{\rm HF}_{\varepsilon\kappa}\,. \tag{2.7}$$

The corresponding correction to the phase shift $\Delta\delta_\kappa(p)$ is shown to be

$$\sin\Delta\delta_\kappa(p) = -\pi\langle\phi^{\rm HF}_{\varepsilon\kappa}|\Sigma_\varepsilon|\phi^{\rm HF}_{\varepsilon\kappa}\rangle\,, \tag{2.8}$$

in the Appendix. The resulting wave function, normalized on the energy scale, is $\phi_{\varepsilon\kappa} = A_{\varepsilon\kappa}\phi^{\rm HF}_{\varepsilon\kappa} + \Delta\phi_{\varepsilon\kappa}$, where the normalization factor is $A_{\varepsilon\kappa} = \cos\Delta\delta_\kappa(p)$. The correlated phase shift is, of course, $\delta_\kappa(p) = \delta^{\rm HF}_\kappa(p) + \Delta\delta_\kappa(p)$.

In our calculations, we approximate $\Sigma_\varepsilon$ by the second-order self-energy $\Sigma^{(2)}_\varepsilon$, which is given in matrix form by the expression

$$[\Sigma^{(2)}_\varepsilon]_{ij} = \sum_{m,n,a}\frac{g_{iamn}(g_{mnja} - g_{mnaj})}{\varepsilon + \varepsilon_a - \varepsilon_m - \varepsilon_n} - \sum_{m,a,b}\frac{g_{imab}(g_{jmab} - g_{mjab})}{\varepsilon_a + \varepsilon_b - \varepsilon_m - \varepsilon}\,, \tag{2.9}$$

and which is illustrated in the Brueckner-Goldstone diagrams of Fig. 1. In Eq. (2.9), the states $a, b, \ldots$ are single-particle states determined in the HF potential of the closed atomic or ionic core. The quantities $\varepsilon_a, \varepsilon_b, \ldots$ are the corresponding HF energies. The quantities $g_{ijkl}$ are two-electron Coulomb matrix elements

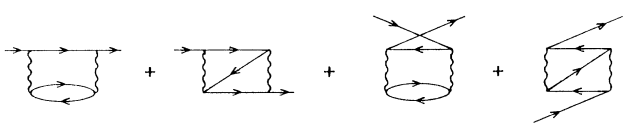

FIG. 1. The four Brueckner-Goldstone diagrams giving the second-order self-energy in Eq. (2.9).

$$g_{ijkl} = \left\langle ij \left| \frac{e^2}{r_{12}} \right| kl \right\rangle . \tag{2.10}$$

The indices $a$ and $b$ in Eq. (2.9) range over the occupied core states, while the indices $m$ and $n$ range over states not occupied in the core. The present relativistic calculations are based on the no-pair Hamiltonian [18–20]; therefore negative energy (positron) states are excluded from the sums in Eq. (2.9).

In lowest approximation, the electron scattering wave function for a given energy $\varepsilon$ and angular momentum $\kappa$ is found by solving the continuum HF equations in the fixed potential of the core. The wave functions are decomposed as products of radial and angular functions,

$$\phi_{\varepsilon\kappa}(\mathbf{r}) = \frac{1}{r} \begin{pmatrix} iP_{\varepsilon\kappa}(r)\Omega_{\kappa m}(\hat{\mathbf{r}}) \\ Q_{\varepsilon\kappa}(r)\Omega_{-\kappa m}(\hat{\mathbf{r}}) \end{pmatrix} , \tag{2.11}$$

where the functions $\Omega_{\kappa m}(\hat{\mathbf{r}})$ are two-component spherical spinors. The continuum wave functions are normalized on the energy scale. Asymptotically, they are given by

$$\begin{pmatrix} P_{\varepsilon\kappa}(r) \\ Q_{\varepsilon\kappa}(r) \end{pmatrix} \to \begin{pmatrix} \sqrt{\frac{\varepsilon+mc^2}{\pi c^2 p}} \cos\left[pr + \nu \ln 2pr + \delta_\kappa + \sigma_\kappa - (\ell+1)\frac{\pi}{2}\right] \\ \sqrt{\frac{\varepsilon-mc^2}{\pi c^2 p}} \sin\left[pr + \nu \ln 2pr + \delta_\kappa + \sigma_\kappa - (\ell+1)\frac{\pi}{2}\right] \end{pmatrix} , \tag{2.12}$$

where $\sigma_\kappa$ is the Coulomb phase shift in the ionic core and $\delta_\kappa$ is the short-range atomic phase shift. The Coulomb phase shift is known analytically; it is given by

$$e^{2i\sigma_\kappa} = \frac{\kappa - i\nu'}{\gamma - i\nu} \frac{\Gamma(\gamma+1-i\nu)}{\Gamma(\gamma+1+i\nu)} e^{-i\pi(\gamma-\ell)} , \tag{2.13}$$

where $\gamma = \sqrt{\kappa^2 - \alpha^2\zeta^2}$, $\alpha = 1/137.035\,989\,5\ldots$ is Sommerfeld's fine-structure constant, and $\zeta$ is the ionic charge. In Eq. (2.13), $\nu = \alpha\zeta\varepsilon/cp$ and $\nu' = \alpha\zeta mc/p$. For xenon, $\zeta = 0$; consequently $\sigma_\kappa = 0$.

In our numerical calculations, we first solve the Hartree-Fock equations and determine the corresponding phase shift $\delta_\kappa^{\rm HF}(p)$. Next, we evaluate the self-energy operator $\Sigma_\varepsilon$. For this purpose, we introduce a finite basis for the HF equation constructed from $B$ splines [21]. The infinite sums and integrals in Eq. (2.9) are thereby reduced to finite sums. Once we have determined $\Sigma_\varepsilon$, we find the second-order correction to the phase shift $\Delta\delta_\kappa(p)$ using Eq. (2.8). In evaluating self-energy from Eq. (2.9), we restrict the sums over occupied states $a$ and $b$ to $5s$ and $5p$ states only. Moreover, we limit the sums over excited states to those having orbital angular momentum $\ell \le 7$.

## III. RESULTS FOR XENON

In Fig. 2, we show the HF and optical-potential phase shifts determined for neutral xenon. As mentioned in the Introduction, both HF and correlated phase shifts at $p = 0$ are multiples of $\pi$, in harmony with Levinson's theorem. In the first panel of the figure, the correlated $s$-wave phase shift is seen to increase from $5\pi$ at threshold to a maximum at $p = 0.12$ a.u., and then to pass through $5\pi$ again at about $p = 0.23$ a.u., leading to a minimum in the cross section at the corresponding energy, $\approx 0.7$ eV. The corrections to $s$-wave and $p$-wave phase shifts are seen to be relatively small; $\approx 0.2$–$0.4$ rad. For the $d$ waves and higher partial waves, on the other hand, the phase shifts at low energies are seen to be dominated by the correlation corrections. This is a consequence of the long range of the electron self-energy operator, which has the asymptotic form $\Sigma_\varepsilon(\mathbf{r},\mathbf{r}') \to -\alpha_d\delta(\mathbf{r}-\mathbf{r}')/2r^4$, where $\alpha_d$ is the dipole polarizability of the core.

In Fig. 3, we show the HF and optical-potential predictions for the cross section as functions of energy. The essential role of correlation in the low-energy cross section is evident from this figure. The HF calculation seriously overestimates the cross section below 3 eV and seriously underestimates it above 5 eV. The cross section is also compared with various experimental measurements [22–24] in the figure. Generally, the agreement between the correlated calculation and experiment is excellent. There are, however, obvious differences below the Ramsauer-Townsend minimum. These differences could be the result of the approximate treatment of correlation here.

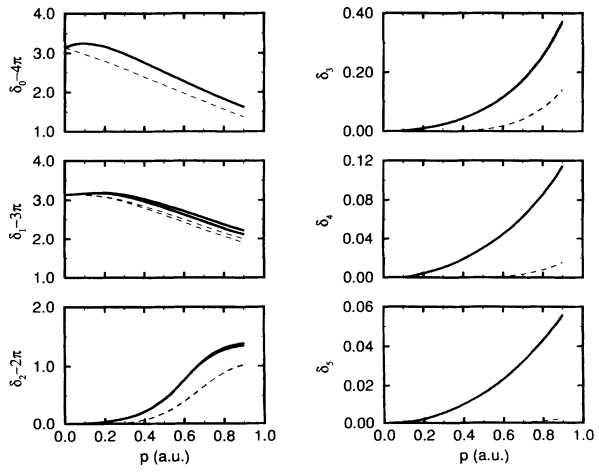


FIG. 2. Optical-potential (solid line) and HF (dashed line) phase shifts for partial waves with $\ell = 0$–$5$ in xenon given as functions of electron momentum. Whenever distinguishable, the upper curve corresponds to the positive value of the relativistic angular momentum $\kappa$ and the lower curve to $\kappa < 0$.

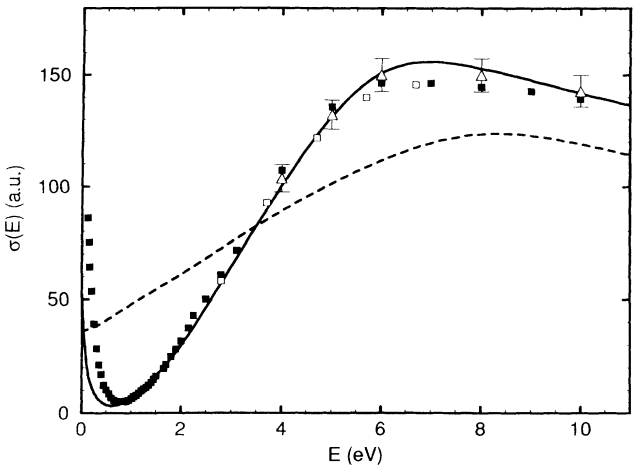


FIG. 3. Optical-potential (solid line) and HF (dashed line) elastic scattering cross sections in xenon as functions of electron energy compared with experiments: full squares [22]; open squares [23]; and open triangles [24].

We compare the differential scattering cross sections at 5 eV and 10 eV calculated using both HF and correlated phase shifts with experiment [25] in Fig. 4. At these energies both the HF and optical-potential cross sections agree qualitatively, but the optical-potential cross section is seen to be in much closer agreement with the measured cross section.

In Fig. 5, a comparison of theory with experiment [26] is given for the Sherman asymmetry function $S(\theta)$ at 5.5 eV and 10 eV. Again there is qualitative agreement between the HF and correlated calculations, but neither calculation is in good quantitative agreement with the measurements, possibly because of experimental inaccuracies [27].

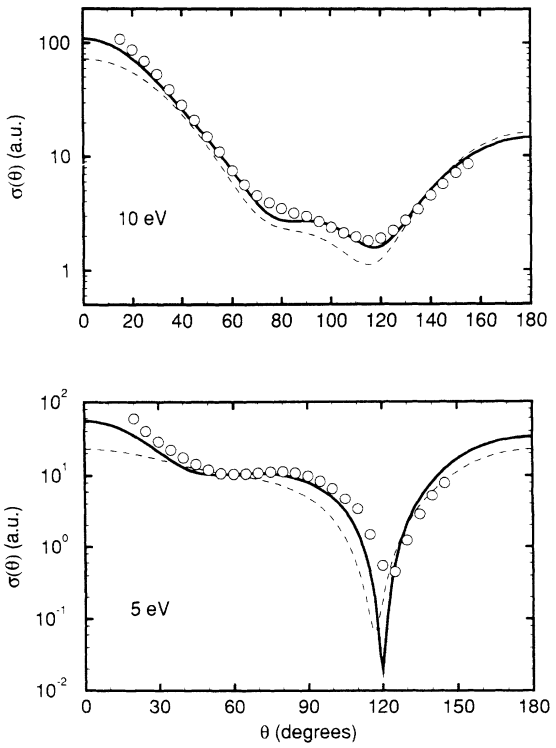


FIG. 4. Optical-potential (solid line) and HF (dashed line) differential scattering cross sections at 5 eV and 10 eV are compared with experiment [25].

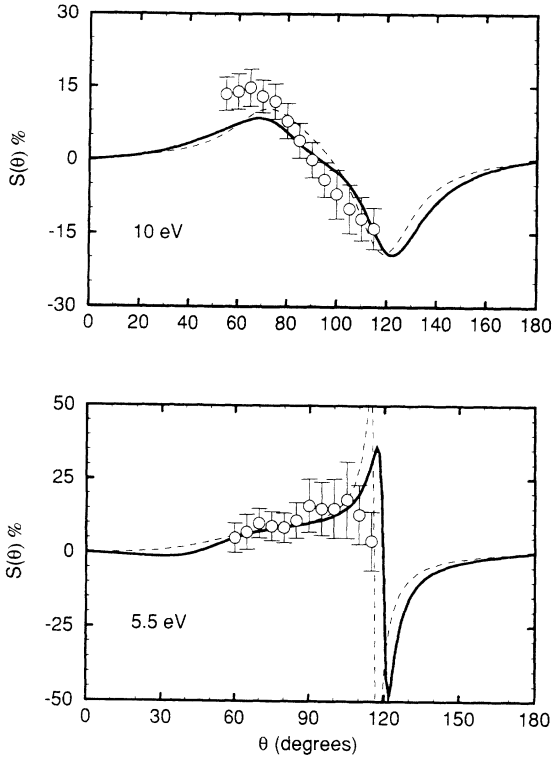


FIG. 5. Sherman asymmetry functions for xenon determined using optical-potential (solid line) and HF (dashed line) phase shifts at 5.5 eV and 10 eV are compared with experiment [26].

To summarize, the optical-potential calculations for xenon lead to total elastic scattering cross sections and differential cross sections in good agreement with experiment below the first inelastic threshold; however, the agreement between the correlated values and experiment for the Sherman asymmetry function is only fair. It is found that the present technique gives a satisfactory account of correlation corrections in low-energy electron-atom scattering. In the next section, we apply this method to electron-ion scattering.

## IV. RESULTS FOR $Cs^+$ AND $Ba^{2+}$

As discussed in Sec. II, the phase shift for a partial wave with angular momentum $\kappa$ is the sum of a Coulomb phase shift $\sigma_\kappa(p)$ and a short-range electron-ion phase shift $\delta_\kappa(p)$. The short-range phase shift, at electron momentum $p = 0$, is related to the quantum defect $\mu_\kappa$ from bound states with angular momentum $\kappa$ by $\delta_\kappa(0) = \pi\mu_\kappa$ [28]. For $Cs^+$, the quantum defects are determined from the observed spectrum of neutral cesium, while for $Ba^{2+}$, the quantum defects are obtained from the $Ba^+$ spectrum

[29]. We list the threshold phase shifts obtained from experimental quantum defects for $Cs^+$ and $Ba^{2+}$ in Table I.

We show the optical-potential phase shifts for $Cs^+$ in Fig. 6 and those for $Ba^{2+}$ in Fig. 7. The threshold phase shifts $\pi\mu_\kappa$ from Table I are indicated by the marks on the left-hand axes of the figures. It is apparent that inclusion of correlation substantially improves the agreement between the calculated phase shifts and those inferred from the quantum defects. The higher partial-wave phase shifts are again dominated by the correlation corrections, as was the case for xenon.

The $f$-wave phase shift for $Ba^{2+}$, which is pathological, requires special attention. The continuum $f$ waves for $Ba^{2+}$ experience a double-well potential, shown in the upper panel of Fig. 8, where we plot the direct part of the HF effective potential and the large components of the $f$-wave functions at electron momenta $p = 0.02, 0.04$, and 0.08 a.u. Low-energy $f$ waves are resonantly trapped in the inner well of this potential, leading to the exceptionally large wave function amplitude in the inner well which is shown in the upper panel of this figure. By contrast, the $f$-wave effective potentials for $Cs^+$ and Xe, shown in the lower two panels of Fig. 8, are seen to have a much shallower inner well and a large centrifugal barrier. The corresponding low-energy $f$ waves are kept well away from the core by the barrier. The resonant trapping of $f$ waves is well known and has been thoroughly investigated in studies of $Ba^{2+}$ photoionization [30,31].

As a consequence of the large overlap of the wave functions with the ionic core, the expression in Eq. (2.8) leads to the result $\sin\Delta\delta_\kappa > 1$ for $f$ states in $Ba^{2+}$. It follows that the treatment of the quasiparticle equation using perturbation theory is no longer valid for these states. If we were solving the quasiparticle equation (2.5) exactly, we would obtain the expression

$$\tan\Delta\delta_\kappa(p) = -\pi\langle\phi^{\rm HF}_{\epsilon\kappa}|\Sigma_\epsilon|\phi_{\epsilon\kappa}\rangle\,, \tag{4.1}$$

rather than Eq. (2.8) for the correlation correction to the phase shift, where $\cos\Delta\delta_\kappa\,\phi_{\epsilon\kappa}(r)$ is assumed to be a solution to Eq. (2.5) normalized on the energy scale. Using Eq. (4.1) with $\phi_{\epsilon\kappa}$ replaced by its lowest approximation, $\phi^{\rm HF}_{\epsilon\kappa}$, leads to the $f$-wave phase shifts shown in the solid curve in Fig. 7. Although the corrections to the HF phase shifts obtained in this way account partially for the difference between the HF phase shifts at threshold and the $Ba^+$ quantum defects, the agreement is unsatisfactory from a quantitative point of view. In the absence of an exact solution to the quasiparticle equation, it is more realistic to treat the correlation corrections

TABLE I. Quantum defects $\pi\mu_\kappa$ for $Cs^+$ and $Ba^{2+}$.

| State | $\kappa$ | $Cs^+$ | $Ba^{2+}$ |
|---|---|---|---|
| $s_{1/2}$ | -1 | 0.18 | -1.32 |
| $p_{1/2}$ | 1 | -1.26 | -2.40 |
| $p_{3/2}$ | -2 | -1.36 | -2.54 |
| $d_{3/2}$ | 2 | 1.46 | 1.24 |
| $d_{5/2}$ | -3 | 1.50 | 1.19 |
| $f_{5/2}$ | 3 | 0.10 | 2.72 |
| $f_{7/2}$ | -4 | 0.10 | 2.60 |

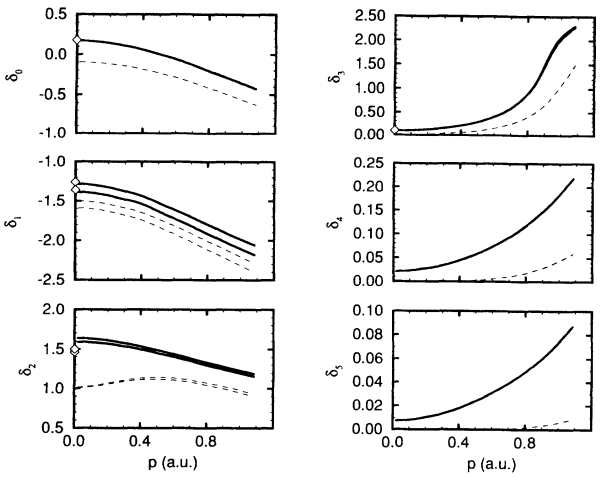


FIG. 6. Optical-potential (solid lines) and HF (dashed lines) phase shifts for partial waves with $\ell = 0$–5 in $Cs^+$. The open diamonds on the left vertical axes mark the values of the quantum defects. Whenever distinguishable, the upper curve corresponds to the positive value of the relativistic angular momentum $\kappa$ and the lower curve to $\kappa < 0$.

for $f$ waves phenomenologically. We do this by adopting a two-parameter model potential for $f$ waves similar to that used in Ref. [11],

$$V = V_{\rm HF} - \frac{\alpha_d r^2}{2(r^3 + r_0^3)^2}\,, \tag{4.2}$$

where $\alpha_d = 10.61a_0^3$ and $r_0 = 1.6a_0$. The value of $\alpha_d$ is taken from a relativistic random-phase approximation (RPA) calculation [32] and the value of $r_0$ is adjusted to give the observed quantum defects. The resulting phenomenological $f$-wave phase shifts are plotted in Fig. 9,

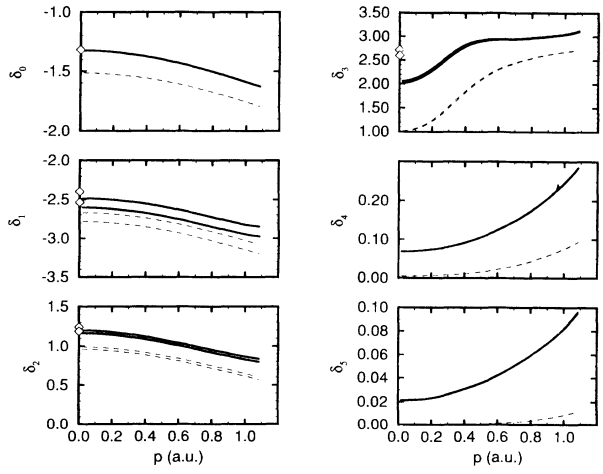


FIG. 7. Optical-potential (solid lines) and HF (dashed lines) phase shifts for partial waves with $\ell = 0$–5 in $Ba^{2+}$. The open diamonds on the left vertical axes mark the values of the quantum defects. Whenever distinguishable, the upper curve corresponds to the positive value of the relativistic angular momentum $\kappa$ and the lower curve to $\kappa < 0$.

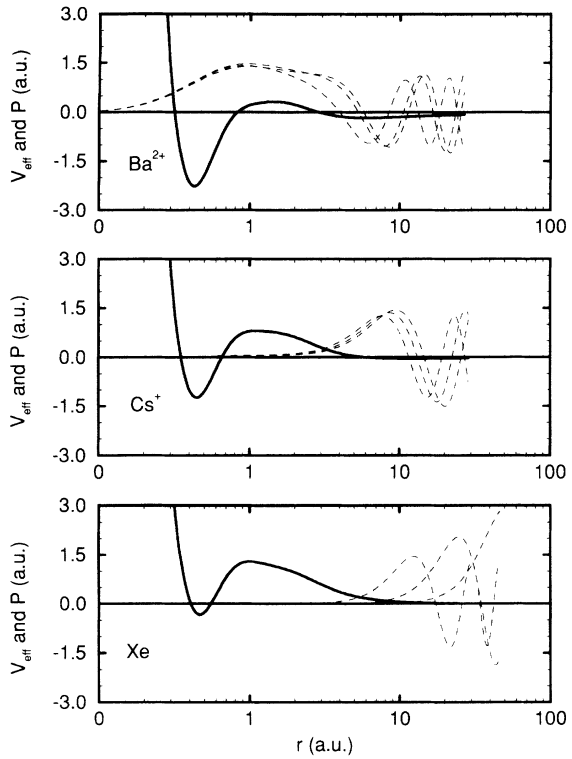


FIG. 8. Effective potential $V_{\rm eff}(r)$ (solid lines) and large components of radial and wave functions $P(r)$ (dashed lines) at $p = 0.02$, 0.04, and 0/08 a.u. for $f$-wave scattering in $Ba^{2+}$, $Cs^{+}$, and Xe.

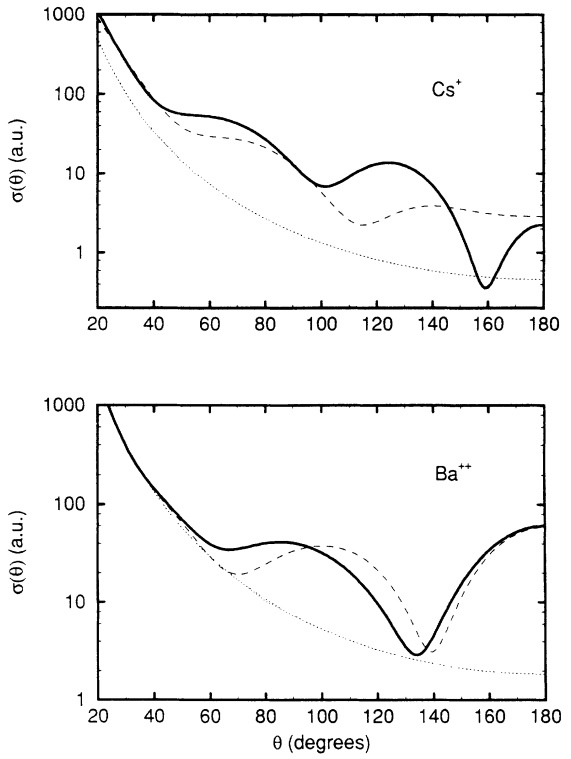


FIG. 10. Differential cross sections for $Cs^{+}$ and $Ba^{2+}$ at 10 eV. Optical-potential (solid line), HF (dashed lines), and Rutherford (dotted lines).

and are used in our subsequent calculations.

Differential cross sections for $Cs^{+}$ and $Ba^{2+}$ at 10 eV are calculated in the HF approximation and with correlation corrections; these cross sections are shown in Fig. 10. Except for forward angles, the correlation corrections lead to marked differences with the HF angular distribution, and both HF and correlated cross sections are substantially different from the Rutherford cross section. The corresponding results for the Sherman asymmetry function are shown in Fig. 11. Correlation corrections are also seen to be important for this quantity.

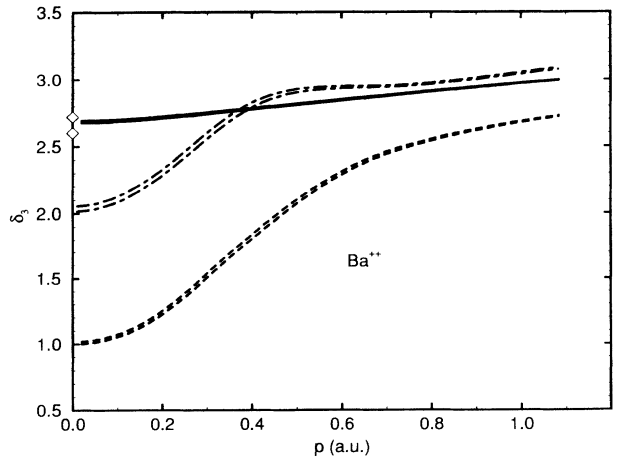


FIG. 9. Phenomenological (solid line), HF (dashed line), and optical-potential (dot-dashed line) $f$-wave phase shifts for $Ba^{2+}$. The open diamonds on the left vertical axis give the values of the phase shifts predicted from quantum defects.

In evaluating these cross sections, the amplitudes $f(\theta)$ and $g(\theta)$ must be treated delicately because of the dominant contributions of the Coulomb field at forward angles. We write $f(\theta) = f^c(\theta) + \Delta f(\theta)$ and $g(\theta) = g^c(\theta) + \Delta g(\theta)$, where $f^c(\theta)$ and $g^c(\theta)$ are Coulomb amplitudes, and where

$$\Delta f(\theta) = \frac{1}{2ip}\sum_{\ell=0}^{\infty}[(\ell+1)(e^{2i\delta_{-\ell-1}}-1)e^{2i\sigma_{-\ell-1}} + \ell(e^{2i\delta_\ell}-1)e^{2i\sigma_\ell}]P_\ell(\cos\theta)\,, \tag{4.3}$$

$$\Delta g(\theta) = \frac{1}{2ip}\sum_{\ell=1}^{\infty}[(e^{2i\delta_{-\ell-1}}-1)e^{2i\sigma_{-\ell-1}} - (e^{2i\delta_\ell}-1)e^{2i\sigma_\ell}]P_\ell^1(\theta)\,. \tag{4.4}$$

The sums in the expressions for $\Delta f(\theta)$ and $\Delta g(\theta)$ converge rapidly, and the Coulomb amplitudes can be replaced by their nonrelativistic limiting forms:

$$f^c(\theta) = \frac{i\nu}{2p\sin^2(\theta/2)}\frac{\Gamma(1-i\nu)}{\Gamma(1+i\nu)}e^{i\nu\ln\sin^2(\theta/2)}\,, \tag{4.5}$$

$$g^c(\theta) = 0\,, \tag{4.6}$$

because of the small value of the ionic charge $\zeta$.

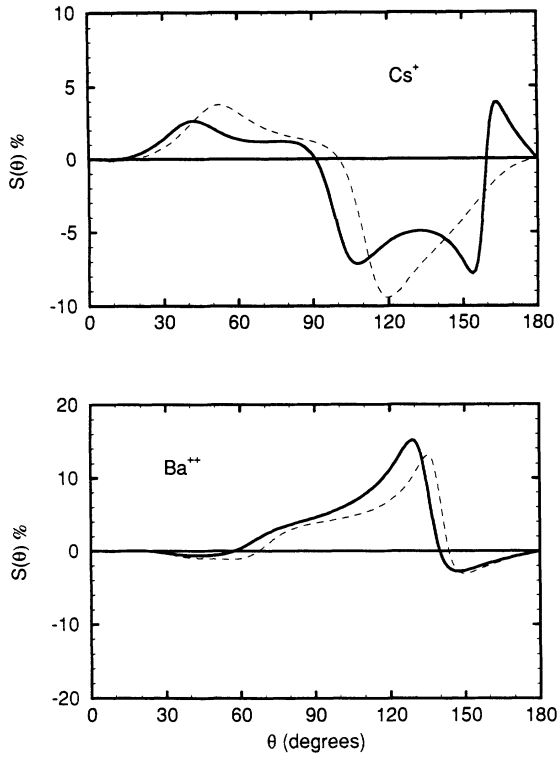


FIG. 11. Sherman asymmetry function for $Cs^+$ and $Ba^{2+}$ at 10 eV. Optical-potential (solid line), HF (dashed lines).

In view of the relative simplicity of the predicted low-energy angular distributions and scattering asymmetry functions for ions (which is due to the absence of resonances at low energies), and because of the relatively large size of correlation corrections, we believe that measurements of low-energy elastic electron-ion scattering will provide interesting tests of atomic many-body theory. We strongly encourage such experiments.

## ACKNOWLEDGMENTS

This work of W.R.J. was supported in part by the National Science Foundation under Grant No. PHY-92-04089. The authors owe debts of gratitude to J. Kessler for supplying as yet unpublished experimental data, to B. Huber for discussions of possible electron-ion scattering experiments, and to M. Amusia for valuable comments on the manuscript.

## APPENDIX: PHASE SHIFTS

The quasiparticle equation (2.5) can be reduced to the following pair of radial Dirac equations:

$$\begin{pmatrix} V_{\rm HF} - \varepsilon_\kappa + mc^2 & c\left(\frac{d}{dr} - \frac{\kappa}{r}\right) \\ -c\left(\frac{d}{dr} + \frac{\kappa}{r}\right) & -\varepsilon_\kappa - mc^2 + V_{\rm HF} \end{pmatrix} \begin{pmatrix} P_\kappa(r) \\ Q_\kappa(r) \end{pmatrix} = \begin{pmatrix} R_\kappa(r) \\ S_\kappa(r) \end{pmatrix}, \quad \text{(A1)}$$

where $[R_\kappa(r), S_\kappa(r)] = -\Sigma_\varepsilon [P_\kappa(r), Q_\kappa(r)]$. With the aid of this equation, one readily establishes the identity

$$\lim_{r\to\infty} c[P_\kappa^{\rm HF}(r)Q_\kappa(r) - Q_\kappa^{\rm HF}(r)P_\kappa(r) = \int_0^\infty [P_\kappa^{\rm HF}(r)R_\kappa(r) + Q_\kappa^{\rm HF}(r)S\kappa(r)]\,dr\,. \quad \text{(A2)}$$

Let us distinguish two cases.

*Case 1.* We solve Eq. (A1) in perturbation theory, replacing the right-hand side by its value in the HF approximation. Assuming that the resulting orbital is normalized on the energy scale as in Eq. (2.12), we obtain from (A2)

$$\sin\Delta\delta_\kappa = -\pi\,\langle\phi_\kappa^{\rm HF}|\Sigma_\varepsilon|\phi_\kappa^{\rm HF}\rangle\,, \quad \text{(A3)}$$

where $\delta_\kappa = \delta_\kappa^{\rm HF} + \Delta\delta_\kappa$.

*Case 2.* We seek a solution to Eq. (A1) having the form

$$\phi_\kappa(r) = \phi_\kappa^{\rm HF}(r) + \Delta\phi_\kappa(r)\,, \quad \text{(A4)}$$

where $\phi_\kappa^{\rm HF}(r)$ is normalized using (2.12). To normalize the resulting function $\phi_\kappa(r)$ on the energy scale, it is necessary to multiply the right-hand side of Eq. (A4) by the factor $\cos\Delta\delta_\kappa$. Again, using the identity (A2) leads to

$$\tan\Delta\delta_\kappa = -\pi\,\langle\phi_\kappa^{\rm HF}|\Sigma_\varepsilon|\phi_\kappa\rangle\,. \quad \text{(A5)}$$

[1] C. Ramsauer, Ann. Phys. (Leipzig) **64**, 513 (1921).
[2] C. Ramsauer and R. Kollath, Ann. Phys. (Leipzig) **12**, 529 (1932).
[3] J.S. Townsend and V.A. Bailey, Philos. Mag. **43**, 593 (1922).
[4] J. Holtzmark, Z. Phys. **55**, 437 (1929).
[5] N.F. Mott, Proc. R. Soc. London, Ser. A **124**, 425 (1929).
[6] R.P. McEachran and A.D. Stauffer, J. Phys. B **17**, 2507 (1984).
[7] R.P. McEachran and A.D. Stauffer, J. Phys. B **19**, 3523 (1986).
[8] R.P. McEachran and A.D. Stauffer, J. Phys. B **20**, 3483 (1987).
[9] Jianmin Yuan and Zhijie Zhang, J. Phys. B **22**, 2581 (1989).
[10] N.T. Padial and W.D. Norcross, Phys. Rev. A **29**, 1742 (1984).
[11] J.E. Sienkiewicz and W.E. Baylis, J. Phys. B **22**, 3733 (1989).
[12] Michael S. Pindzola and Hugh P. Kelly, Phys. Rev. A **9**, 323 (1974).
[13] M.Ya. Amusia, N.A. Cherepkov, L.V. Chernysheva, and

S.G. Shapiro, Phys. Lett. **46A**, 387 (1974).
[14] M.Ya. Amusia, N.A. Cherepkov, S.G. Shapiro, and A. Tančić, Zh. Eksp. Teor. Fiz. **68**, 2023 (1975) [Sov. Phys. JETP **41**, 1012 (1975)].
[15] V.B. Berestetskii, E.M. Lifshitz, and L.P. Pitaevskii, *Quantum Electrodynamics*, 2nd ed. (Pergamon Press, Oxford, 1982), p. 140.
[16] J. Kessler, *Polarized Electrons* (Springer, Berlin, 1985), Chap. 3.
[17] A.B. Migdal, *Theory of Finite Fermi-Systems and Properties of Atomic Nuclei* (Nauka, Moscow, 1983).
[18] G.E. Brown and D.G. Ravenhall, Proc. R. Soc. London, Ser. A **208**, 502 (1951).
[19] J. Sucher, Phys. Rev. A **30**, 703 (1980).
[20] M.H. Mittleman, Phys. Rev. A **4**, 893 (1971); **5**, 2395 (1972); **24**, 1167 (1981).
[21] W.R. Johnson, S.A. Blundell, and J. Sapirstein, Phys. Rev. A **37**, 307 (1988).
[22] J. Ferch, F. Simon, and G. Strakeljahn (unpublished).
[23] M.S. Dababneh, W.E. Kauppila, J.P. Downing, F. Laperriere, V. Pol, J.H. Smart, and T.S. Stein, Phys. Rev. A **22**, 1872 (1980).
[24] J.C. Nickel, K. Imre, D.K. Register, and S. Trajmar, J. Phys. B **18**, 125 (1985).
[25] J. Kessler (private communication).
[26] M. Klewer, M.J. Beerlage, and M.J. van der Wiel, J. Phys. B **12**, 3935 (1979).
[27] C. Garcia-Rosales, H. Müller, and J. Kessler, J. Phys. B **21**, L477 (1988).
[28] W.R. Johnson and K.T. Cheng, J. Phys. B **12**, 863 (1979).
[29] C.E. Moore, *Atomic Energy Levels*, Natl. Bur. Stand. Ref. Data Ser., Natl. Bur. Stand. (U.S.) Circ. No. 35 (U.S. GPO, Washington, DC, 1971), Vol. III.
[30] J.P. Connerade, J. Phys. B **16**, L257 (1983).
[31] K.T. Cheng and C. Froese Fischer, Phys. Rev. A **28**, 2811 (1983).
[32] W.R. Johnson and D. Kolb, At. Data Nucl. Data Tables **28**, 333 (1983).